International Journal of Fracture (2005) 132:249–273
DOI 10.1007/s10704-005-2182-1 © Springer 2005

Analysis of temperature effects near mode I cracks in glassy polymers

R. ESTEVEZ[1,*], S. BASU[2] and E. VAN DER GIESSEN[3]
[1]*INSA Lyon, GEMPPM, 20 Av A Einstein, Bât. St Exupéry, 69621 Villeurbanne, Cedex, France*
[2]*Department of Mechanical Engineering, Indian Institute of Technology Kanpur, Kanpur 208016, India*
[3]*Materials Science Center – Micromechanics of materials, University of Groningen, Nijenborgh 4, 9749 AG, Groningen, The Netherlands*
[*]*Author for correspondence (E-mail: rafael.estevez@insa-lyon.fr)*

Received 15 September 2004; accepted in revised form 14 February 2005

Abstract. A previous isothermal study (Estevez et al., *Journal of Mechanics and Physics of Solids* **48**, 2585–2617, 2000) has shown that the toughness of glassy polymers is governed by the competition between shear yielding and crazing. The present work aims at investigating loading rates for which thermal effects need to be accounted for. The influence of the heat coming from the viscoplastic shear yielding and from crazing on their competition and on the toughness is examined. Crazing is shown to be the dominant heat source, and the dependence of the craze properties on temperature appears to be key in controlling the toughness of the material.

Key words: Cohesive surface, crack tip plasticity, crazing, elastic-viscoplastic material, fracture, polymer, temperature.

1. Introduction

Studies of temperature effects during fracture of glassy polymers aim at investigating how the toughness varies with loading rates (e.g. Döll, 1973, 1976; Fuller et al., 1975). Plastic dissipation during the fracture process is converted into heat, the measure of which can be correlated with the energy release rate (Döll, 1976). Döll (1973) has argued that the heat originates from localized plastic dissipation ahead of the crack tip, within a Dugdale zone. This picture is consistent with early evidence of crazing as the mechanism for fracture in glassy polymers (Kambour, 1973) and with the traces of crazes along the fracture surface of PMMA observed by Fuller et al. (1975) for a crack speed up to 300 m/s. For higher crack velocities (observed up to 650 m/s,) the fracture surfaces become rougher and no evidence of crazes is available. Although clearly observed for cracks running at speeds up to 300 m/s, crazing was assumed to operate for any crack velocity and serves as the only heat source by Fuller et al. (1975). These authors also report a steady increase of heat generated with crack speed. The increase of the amount of heat is accompanied by an increase of the temperature which is estimated by Döll (1973) and Fuller et al. (1975) to be hundreds of Kelvins. Recently, Bjerke and Lambros (2003) have reported estimates of the temperature increase from infrared measurements. Their study suggest that the temperature rise is not as large but about one hundred Kelvins. The discrepancy is likely to come from the intermediate analysis of the experimental data of Döll (1973) and Fuller et al. (1975).

The fracture of glassy polymers shows a marked increase of the toughness in the transient regime between static and dynamic conditions. This has been observed by Williams and Hodgkinson (1981) for various polymers with Charpy tests in which different loading rates are prescribed by changing the dimensions of the specimen and the speed of the impact striker. The measured energy release rate G_c shows a noticeable increase for loading times till fracture of about 0.2 ms. In studies devoted to the analysis of the dynamic fracture of PMMA (Wada, 1992; Wada et al., 1996; Rittel and Maigre, 1996), a similar feature is observed for loading rates around $\dot{K}_I = 10^4\,\mathrm{MPa}\sqrt{\mathrm{m}}/\mathrm{s}$. By combining the experimental results with FEM calculations, an estimate of the dynamic toughness of a few $\mathrm{MPa}\sqrt{\mathrm{m}}$ is derived, which is consistent with the results reported by Williams and Hodgkinson (1981).

The above mentioned increase in toughness corresponds to a second transition *opposite* to the classical ductile-to-brittle transition operating at lower rates. This second one is observed for intermediate loading rates, between quasi-static and dynamic conditions, for which thermal effects become important. Temperature variations are thought to occur prior to crack propagation from plastic conversion into heat (Williams and Hogdkinson, 1981) but also from thermoelastic cooling as reported by Rittel (1998).

The present investigation aims at exploring the variations of the toughness with loading rate of glassy polymers when temperature effects need to be accounted for. It is now established that their failure involves both shear yielding and crazing. Shear yielding is the typical high-stress inelastic response of glassy polymers featuring softening upon yielding followed by progressive hardening. Crazing also involves some plasticity during the thickening of craze fibrils, but this takes place at a smaller size scale. A previous analysis (Estevez et al., 2000) has used a small-scale yielding model to investigate the influence of these two mechanisms on the fracture toughness. Shear yielding is incorporated through a viscoplastic model, while a cohesive surface is used to describe crazing. Although restricted to isothermal conditions, it was demonstrated that the predicted fracture toughness for a given loading rate is governed by the competition between the natural time scales of both mechanisms.

The extension of the above-mentioned work to a coupled thermo-mechanical analysis is necessary to study loading rates at which the isothermal assumption does not hold anymore. The coupled thermo-mechanical framework used here has been detailed in (Basu and Van der Giessen, 2002) for a study on stationary crack tip fields for mode I loading. This study is extended here to incorporate crack growth by crazing, including the plastic dissipation involved in the crazing process and its conversion to heat. The temperature rise at the crack tip can originate from plasticity in the bulk material and plastic dissipation during the crazing process. The consequences of the temperature variation on shear yielding and crazing, and their influence on the fracture toughness are investigated.

Tensors are denoted by bold-face symbols, $\otimes$ is the tensor product and $\cdot$ the scalar product. For example, with respect to a Cartesian basis $\boldsymbol{e}_i$, $\boldsymbol{A}\boldsymbol{B} = A_{ik}B_{kj}\boldsymbol{e}_i \otimes \boldsymbol{e}_j$, $\boldsymbol{A}\cdot\boldsymbol{B} = A_{ij}B_{ij}$ and $\mathcal{L}\boldsymbol{B} = \mathcal{L}_{ijkl}B_{kl}\boldsymbol{e}_i \otimes \boldsymbol{e}_j$, with summation implied over repeated Latin indices. The summation convention is *not* used for repeated Greek indices. A prime $(\,)'$ identifies the deviatoric part of a second-order tensor, $\boldsymbol{I}$ is the second-order unit tensor and tr denotes the trace.

2. Constitutive law for amorphous polymers

When crazing does not take place or is suppressed, as in compression or shear tests, amorphous glassy polymers can undergo quite large strains (up to about 100%). Their response shows softening upon yielding followed by progressive hardening as the deformation continues. In a numerical investigation of inelastic deformation and localization in polycarbonate, Lu and Ravi-Chandar (1999) pointed out that macroscopic softening of the specimen does not necessarily imply softening to be an intrinsic property of the material. However, in an analysis of the stress and strain fields around the tip of a blunted crack under mode I, Lai and Van der Giessen (1997) showed that intrinsic softening is necessary to capture the localized strain fields observed experimentally as in (Ishikawa et al., 1977).

We start out with the constitutive description of amorphous polymers at large plastic strains for temperatures below the glass transition T_g, postponing that for $T \geqslant T_g$ for the moment. The constitutive model is based on the formulation of Boyce et al. (1988) but we use a modified version introduced by Wu and Van der Giessen (1993). Details of the governing equations and the computational aspects can be found in Wu and Van der Giessen, (1996). The reader is also referred to the review by Van der Giessen (1997) together with a presentation of the thermo-mechanical framework in Basu and Van der Giessen (2002).

The constitutive model makes use of the decomposition of the rate of deformation $\boldsymbol{D}$ into an elastic $\boldsymbol{D}^e$ and a plastic part $\boldsymbol{D}^p$ as $\boldsymbol{D} = \boldsymbol{D}^e + \boldsymbol{D}^p$. Prior to yielding, no plasticity takes place and $\boldsymbol{D}^p = 0$. In this regime, most amorphous polymers exhibit visco-elastic effects but these are neglected here since we are primarily interested in the effect of the bulk plasticity. Assuming the elastic strains and the temperature differences (relative to a reference temperature T_0) to remain small, the thermo-elastic part of the response is taken to be governed by

$$\overset{\triangledown}{\boldsymbol{\sigma}} = \mathcal{L}_e \boldsymbol{D}^e - C\alpha_c \dot{T}\boldsymbol{I}, \tag{1}$$

where $\overset{\triangledown}{\boldsymbol{\sigma}}$ is the Jaumann rate of the Cauchy stress and $\boldsymbol{\mathcal{L}}_e$ the usual fourth-order isotropic elastic modulus tensor. The parameters C and α_c are the bulk modulus and the coefficient of cubic thermal expansion. Assuming that the yield response is isotropic, the isochoric visco-plastic strain rate

$$\boldsymbol{D}^p = \frac{\dot{\gamma}^p}{\sqrt{2}\,\tau}\bar{\boldsymbol{\sigma}}', \quad \text{with } \tau = \sqrt{\tfrac{1}{2}\bar{\boldsymbol{\sigma}}' \cdot \bar{\boldsymbol{\sigma}}'} \tag{2}$$

is specified in terms of the equivalent shear strain rate $\dot{\gamma}^p = \sqrt{\boldsymbol{D}^p \cdot \boldsymbol{D}^p}$, the driving stress $\bar{\boldsymbol{\sigma}} = \boldsymbol{\sigma} - \boldsymbol{b}$ and the related equivalent shear stress τ. The back stress tensor $\boldsymbol{b}$ describes the progressive hardening of the material as the strain increases and will be defined later on. The equivalent shear strain rate $\dot{\gamma}^p$ is taken from Argon's (1973) expression

$$\dot{\gamma}^p = \dot{\gamma}_0 \exp\left[-\frac{As_0}{T}\left\{1 - \left(\frac{\tau}{s_0}\right)^{5/6}\right\}\right] \quad \text{for } T < T_g, \tag{3}$$

where $\dot{\gamma}_0$ and A are material parameters and T the absolute temperature. Argon's model is based on the notion that shear yielding below T_g originates from the motion

of molecular segments through a thermally activated kinking process (note that plastic flow is inherently temperature dependent). The shear strength s_0 in Equation (3) is related to elastic molecular properties in Argon's original formulation but is considered here as a separate material parameter. It has been found in a number of works to give a fair description of rate and temperature yield of polymers including PMMA (Arruda et al., 1995), SAN (Steenbrink and Van der Giessen, 1999) and PC (Boyce and Arruda, 1990). In order to account for the effect of strain softening and for the pressure dependence of the plastic strain rate, s_0 in (3) is replaced by $s+\alpha p$, where α is a pressure sensitivity coefficient and $-p=(1/3)\mathrm{tr}\ \boldsymbol{\sigma}$. The shear strength s is taken to evolve from the initial value s_0 with the plastic strain rate through

$$\dot{s}=h(1-s/s_{\mathrm{ss}})\dot{\gamma}^{\mathrm{p}} \tag{4}$$

as a simple way to incorporate strain softening. Here, h controls the rate of softening while s_{ss} represents the final, steady state value of s. The energy dissipation rate per unit volume $\dot{\mathcal{D}}$ is given by

$$\dot{\mathcal{D}}=\bar{\boldsymbol{\sigma}}'\cdot\boldsymbol{D}^{\mathrm{p}}=\sqrt{2}\,\tau\dot{\gamma}^{\mathrm{p}}\,. \tag{5}$$

The resulting temperature rise will be accounted for in the coupled analysis to be presented later on. As discussed in more detail by Basu and Van der Giessen (2002), Equation (5) emphasizes that only part of the plastic work $\boldsymbol{\sigma}'\cdot\boldsymbol{D}^{\mathrm{p}}$ in amorphous polymers is dissipated; the rest, $\boldsymbol{b}'\cdot\boldsymbol{D}^{\mathrm{p}}$, is stored in the distorted network.

Completion of the constitutive model requires the description of the progressive hardening of amorphous polymers upon yielding due to deformation-induced stretch of the molecular chains. This effect is incorporated through the back stress $\boldsymbol{b}$ in the driving shear stress τ in Equation (2). Its description is based on the analogy with the stretching of the cross-linked network in rubber elasticity, but with the cross-links in rubber being replaced with the physical entanglements in a flowing amorphous glassy polymer (Boyce et al., 1988). The deformation of the resulting network is assumed to derive from the accumulated plastic stretch (Wu and Van der Giessen, 1993) so that the principal back stress components b_α are functions of the principal plastic stretches λ_β as

$$\boldsymbol{b}=\sum_{\alpha} b_\alpha(\boldsymbol{e}_\alpha^{\mathrm{p}}\otimes\boldsymbol{e}_\alpha^{\mathrm{p}})\,,\quad b_\alpha=b_\alpha(\lambda_\beta)\,,$$

in which $\boldsymbol{e}_\alpha^{\mathrm{p}}$ are the principal directions of the plastic stretch. In a description of the fully three-dimensional orientation distribution of non-Gaussian molecular chains in a network, Wu and Van der Giessen (1993) showed that $\boldsymbol{b}$ can be estimated accurately with the following combination of the classical three-chain model and the eight-chain description of Arruda and Boyce (1993)

$$b_\alpha=(1-\rho)b_\alpha^{3-\mathrm{ch}}+\rho b_\alpha^{8-\mathrm{ch}}\,, \tag{6}$$

where the fraction $\rho=0.85\bar{\lambda}/\sqrt{N}$ is based on the maximum plastic stretch $\bar{\lambda}=\max(\lambda_1,\lambda_2,\lambda_3)$ and on N, the number of segments between entanglements. The use of Langevin statistics for calculating b_α implies a limit stretch of $\sqrt{N}$. The expressions for the principal components of $b_\alpha^{3-\mathrm{ch}}$ and $b_\alpha^{8-\mathrm{ch}}$ contain a second material

parameter: the initial shear modulus $C^R = nkT$, in which n is the volume density of entanglements (k is the Boltzmann constant).

Based on a study of the temperature dependence of strain-induced birefringence in amorphous polymers, Raha and Bowden (1972) suggested that the thermal dissociation of entanglements can be described by

$$n(T) = B - D\exp(-E_a/RT), \tag{7}$$

where E_a is the dissociation energy, R the gas constant, and where B and D are material constants. As pointed out by Arruda et al. (1995), this evolution law is subject to the side condition $nN = \text{constant}$ in order to keep the number of molecular links constant. Therefore, the back stress according to (6) is also temperature dependent through $N(T)$ and $C^R = n(T)kT$. The material parameters B and D are estimated here from the assumption that the back stress vanishes as the temperature approaches T_g, resulting in $n(T_g) = 0$ so that $B/D = \exp(-E_a/RT_g)$.

The formulation above is assumed to hold for temperatures up to the glass transition T_g. In an earlier preliminary study, Estevez et al. (2000b) observed that locally the temperature can reach T_g at quite early stages of the crack propagation. The area affected by such a large temperature increase was concentrated at the craze-crack interface of a running crack, over a region of the order of a micron. When this situation was encountered, the calculations were aborted thus restricting the loading range under investigation.

In order to overcome this, the constitutive law is extended here with a formulation of the material response for $T > T_g$. Most studies found in the literature focus on the description of the molten state (Agassant et al., 1991) due to its practical importance while little attention is paid to the response of glassy polymers in the rubbery state, near T_g. The mechanical response of molten material is Newtonian for low strain rates ($\dot{\gamma} < 1\,s^{-1}$) and non-Newtonian (pseudo-plastic) for strain rates larger than $1\,s^{-1}$. One of the most common non-Newtonian models is of the form $\tau = \eta\dot{\gamma}^m$, where m and η are material parameters with η being also temperature dependent. For the loading rates to be considered in the present work, we will assume that this non-Newtonian response prevails as soon as T_g is exceeded by replacing (3) with

$$\dot{\gamma}^p = \varkappa\dot{\gamma}_0\left(\frac{\tau}{s_0}\right)^{1/m} \quad \text{for } T > T_g. \tag{8}$$

In this expression, η has been substituted for convenience by $s_0/(\varkappa\dot{\gamma}_0)^m$, with s_0 and $\dot{\gamma}_0$ being below-T_g parameters in (3), and $\varkappa$ a non-dimensional constant. The deformation in the molten state is generally believed to involve chain slippage and temporary entanglements between the moving chains resulting in the non-Newtonian viscosity (Agassant et al., 1991). The details of the deformation process are lumped into the parameters η (or $\varkappa$) and m so that no back stress contribution appears above T_g.

The exponent m is observed to vary between 0.3 and 1 for molten polymers (Agassant et al., 1991) but for those exhibiting a marked non-Newtonian response like most glassy polymers, m ranges from 0.3 to 0.5; the value of 0.4 is adopted. For a given temperature, the variation of the viscosity η with increasing strain rate is observed to decrease from a Newtonian value η_0 at low strain rates to a level

five or six decades smaller (Van Krevelen, 1990; Agassant et al., 1991). For a temperature around T_g, the value of η_0 can be estimated from (Van Krevelen, 1990) to be of the order of some MPa's for materials like PMMA or PC. A smaller value is expected in the non-Newtonian regime so that for temperatures above T_g a constant value of $\eta = 0.35$ MPa ($\varkappa = 0.02$) is used to describe the material response in the molten state. With this simple description, we only aim at being able to continue our calculations if the temperature exceeds T_g locally, when the crack propagates. We need to keep in mind that we are primarily concerned with temperatures below T_g and the incorporation of more sophisticated models as found in (Van Krevelen, 1990; Agassant et al., 1991) is out of the scope of the present investigation.

Figure 1 shows the material's response for uniaxial tension that is obtained with the constitutive model described above under adiabatic conditions, i.e. when all the dissipated energy, defined in Equation (5), is converted into a temperature rise. The material parameters used are given in Table 1 and are representative of SAN in the glassy state. The parameters of SAN have been adopted since its response is intermediate between that of PMMA which exhibits a higher yield stress under compression and an early failure under tension and that of polycarbonate which deforms plastically for a lower yield stress than SAN and PMMA in compression and which is one of the most ductile glassy polymers under tension. The thermal properties reported in Table 2 are borrowed from (Basu and Van der Giessen, 2002). These are not varying noticeably for most of the glassy polymers so that the parameters of Table 2 are thought to be representative of the thermal properties of this class of materials. Before the glass transition temperature is attained, the constitutive response is given by Equation (3) while beyond the glass transition temperature, it switches to Equation (8). At strain rates of $10^2\,s^{-1}$ and $10^4\,s^{-1}$, the material abruptly loses almost all its stress carrying capacity as soon as the glass transition temperature is reached. However, at even higher strain rates of $10^6\,s^{-1}$, the flow strength of the melt remains comparable to that of the solid.

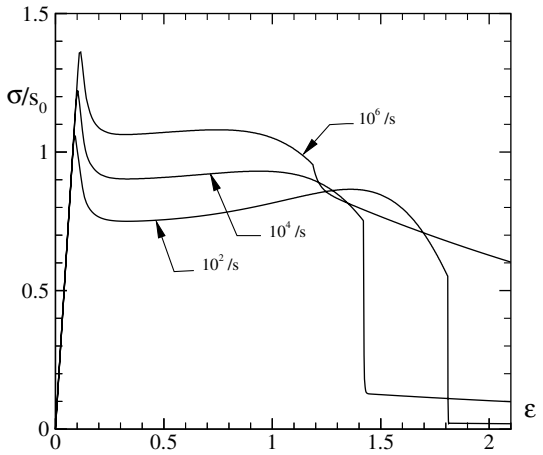

Figure 1. Stress (σ)– strain (ε) response of the bulk material for a uniaxial tension at different strain rates with the parameters of Table 1.

Table 1. The set of bulk parameters used in this study, representative of SAN at room temperature with $s_0 = 120$MPa (Steenbrink and Van der Giessen, 1999) supplemented with $\varkappa$ and m involved in the description for $T > T_g$ in Equation (8).

$\dot{\gamma}_0(s^{-1})$	E/s_0	ν	s_{ss}/s_0	As_0/T	h/s_0	α	N	C^R/s_0	$\varkappa$	m
1.06×10^8	12.6	0.38	0.79	52.2	12.6	0.25	12.0	0.033	0.02	0.4

Table 2. The set of parameters used in the thermal part of the analysis (Basu and Van der Giessen, 2002).

E_a/R	k	α_c	ρ	c_v	T_g
2.8×10^3 K	0.35 W/mK	2×10^{-4} K^{-1}	1.08×10^3 kg/m^3	1.38×10^3 J/kgK	383 K

3. Craze modelling

Failure of glassy polymers is assumed to originate from crazing. A craze appears geometrically similar to a crack but the craze surfaces are bridged by a web of polymer fibrils which provide some load-bearing capacity, in contrast to the traction-free faces of a crack. Crazing proceeds in three stages: (1) initiation; (2) thickening of the craze fibrils; (3) breakdown of the fibrils and nucleation of a crack. We adopt a model of crazing within the framework of a cohesive zone which has been initiated by Tijssens et al. (2000). The reader is referred to this reference together with (Estevez et al., 2000) for details of the formulation.

Following the experimental study by Sternstein and Ongchin (1969) and under plane strain conditions, crazing is taken to be initiated when

$$\sigma_n \geq \sigma_m - \frac{A^0}{2} + \frac{B^0}{6\sigma_m}, \tag{9}$$

in which σ_n is the stress normal to the plane of initiation and $\sigma_m = (1/3)\,\mathrm{tr}\,\boldsymbol{\sigma}$ is the mean stress. The coefficients A^0 and B^0 are material parameters and possibly temperature dependent (Sternstein and Myers, 1973). As crazes appear perpendicular to the direction of maximal principal stress, the condition (9) is checked throughout the material by taking the local maximum principal stress as σ_n.

Based on Kramer's description (1983, 1990), the growth of craze fibrils involves plastic flow, concentrated within a thin layer between the fibrils and the bulk. Motivated by this, we take the thickening of a craze, i.e. the lengthening of the fibrils, to be governed by an expression similar to Equation (3) (Tijssens et al., 2000; Estevez et al., 2000)

$$\dot{\Delta}_n^c = \dot{\Delta}^0 \exp\left[\frac{-A^c\sigma^c}{T}\left\{1 - \frac{\sigma_n}{\sigma^c}\right\}\right], \tag{10}$$

where $\dot{\Delta}_0$, A^c and σ^c are material parameters (σ^c is the athermal stress for craze thickening). Thus, the thickening rate of the craze is temperature and time dependent. Although initially developed for the analysis of craze thickening at temperatures

below the glass transition T_g, the formulation of the craze growth rate in Equation (10) is assumed to remain valid above T_g, during the propagation of the crack. Thus, we neglect the possible contribution from chain disentanglement to the craze thickening when the temperature is close to T_g. Once crazing has initiated, the thickening process continues until Δ_n^c reaches a critical thickness $\Delta_n^{c\,cr}$, a material parameter that primarily depends on the molecular weight.

The complete traction–separation law used to describe crazing is

$$\dot{\sigma}_n = k_n \left(\dot{\Delta}_n - \dot{\Delta}_n^c \right) , \tag{11}$$

in which $\dot{\Delta}_n$ is the prescribed thickening rate on the craze surface, $\dot{\Delta}_n^c$ is the craze thickening rate from Equation (10) once the craze initiation criterion (9) is satisfied. When the condition $\Delta_n^c = \Delta_n^{c\,cr}$ is attained, the related crack nucleation is accounted for by prescribing $\sigma_n = 0$ at the location of fibrils breakdown along the cohesive zone.

Figure 2 gives a schematic traction-thickening response of a craze to a constant thickening rate $\dot{\Delta}_n$ in accordance with Equation (11). In the regime [1], crazing has not yet initiated and the increase of σ_n results in a small reversible opening of the cohesive surface, controlled by the elastic stiffness k_n in (11). Once craze initiation has taken place, the craze widens and depending on the stress state prior to craze initiation and the prescribed thickening rate $\dot{\Delta}_n$, a transient [2a] hardening or [2b] softening takes place prior to fibrillation at approximately constant normal stress. This process continues up to point [3] where the condition of craze breakdown is reached and a crack is formed locally.

As a craze thickens, the related energy dissipation is accounted for through the viscoplastic thickening rate (10). Within a two-dimensional cohesive zone representation of a craze, the heat generated during the craze thickening process is accounted for by defining a heat flux over the cohesive surface, as will be discussed in the next section.

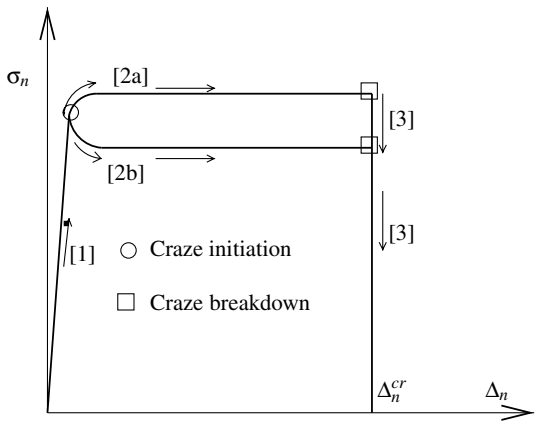

Figure 2. Schematic representation of the cohesive surface traction–opening law: [1] no crazing, [2] craze thickening for either a hardening (a) or a softening (b) response, [3] craze fibril breakdown at $\Delta_n = \Delta_n^{cr}$ and subsequent crack formation.

4. Problem formulation

Like Estevez et al. (2000), we perform a plane strain, small-scale yielding analysis of mode I crack growth in a homogeneous polymer. The crack is initially blunted with a tip radius r_t. Crazing is restricted to take place along the crack symmetry plane and we exploit the symmetry of the problem to analyse only half of the geometry (see Figure 3). Within a standard small-scale yielding framework, loading is applied via the mode I elastic K field prescribed at the remote boundary, and positioned at a distance $R = 200 r_t$ from the crack tip. The mesh has been designed and verified to be able to accurately capture the emerging localized fields.

The formulation is extended here to account for thermal effects associated with the heat generated by plastic dissipation in the bulk and from the craze process. With the bulk plastic dissipation being given by (5), the energy balance inside the material can be written as

$$\rho c_v \dot{T} = k \nabla^2 T + \bar{\boldsymbol{\sigma}}' \cdot \boldsymbol{D}^p \tag{12}$$

with k the isotropic heat conductivity in accordance with Fourier's law, ρ the mass density and c_v the specific heat.

There is a second source of energy dissipation, namely the fibrillation process during craze thickening, as described in Section 3. Per unit of area, the rate of dissipation amounts to $\sigma_n \dot{\Delta}_n^c$ and, in the cohesive surface methodology, represents a heat flux $\boldsymbol{q} = k \nabla T$ into the system through the surface of the craze. When crazing has not yet initiated, there is no heat flux across the symmetry plane $x_2 = 0$. The energy balance (12) thus becomes subject to the following boundary condition on the cohesive surfaces:

$$\frac{\partial T}{\partial x_2} = \begin{cases} 0 & \text{on } x_2 = 0, \text{ without a craze,} \\ \frac{1}{2}\sigma_n \dot{\Delta}_n^c / k & \text{on } x_2 = \pm \frac{1}{2}\Delta_n(x_1), \text{along the craze surfaces,} \end{cases} \tag{13}$$

where Δ_n is the thickness along the cohesive surface ahead of the crack (the factor 1/2 is due to symmetry). All other boundaries are assumed to be insulated. For this

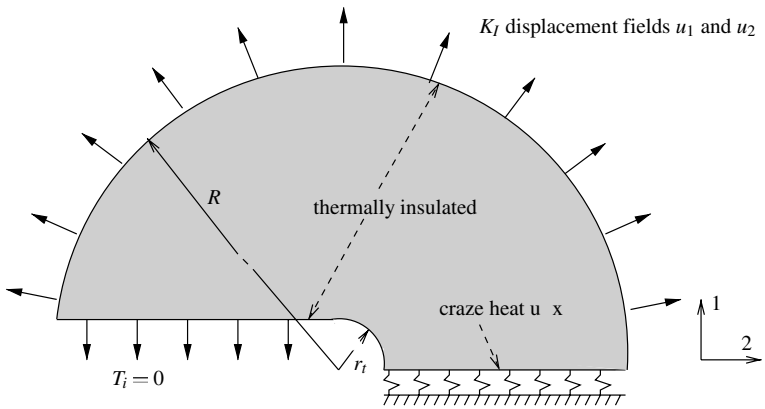

Figure 3. Schematic representation of the problem formulation and boundary conditions for the coupled thermal and mechanical analysis.

Table 3. The set of craze parameters used in this study (case 8 in Estevez et al., 2000).

A^0/s_0	$B^0/(s_0)^2$	Δ_n^{ccr}/r_t	σ^c/s_0	$A^c\sigma^c/T$	$\dot{\Delta}^0/r_t(s^{-1})$
0.68	1.4	0.1	0.83	136.5	100

second source of heat, we assume that the heat flux originates from the full conversion of the plastic work $\sigma_n\dot{\Delta}_n^c$ involved in the craze widening process. In this case, the fraction of the energy that remains blocked by the craze structure is difficult to estimate and the assumption of a full conversion in the definition of the heat flux in (13) provides an upper bound for the estimate of the temperature variations.

The heat Equation (12) is coupled to the equations governing the mechanical response through the temperature dependence of the bulk viscoplastic strain rate (3), the craze thickening rate (10) and the thermal expansion in (1). A quasi-static finite strain analysis which uses a total Lagrangian description for the continuum field equations is carried out while the cohesive surface is analyzed in the current configuration. The virtual work rate expression for this problem then reads

$$\int_V \boldsymbol{\tau}\cdot\delta\dot{\boldsymbol{\eta}}\,\mathrm{d}V+\int_{S_{cz}}\sigma_n\delta\dot{\Delta}_n\,\mathrm{d}S=\int_{\partial V}\boldsymbol{T}\cdot\delta\boldsymbol{v}\,\mathrm{d}S \tag{14}$$

with V and ∂V denoting the volume of the region in the initial configuration and its boundary, respectively, and where S_{cz} is the cohesive surface in the current state. In (14), $\boldsymbol{\tau}$ is the second Piola–Kirchhoff stress tensor, $\boldsymbol{T}$ the corresponding traction vector; $\dot{\boldsymbol{\eta}}$ and $\boldsymbol{v}$ are the conjugate Lagrangian strain rate and velocity. The governing equations are solved in a linear incremental fashion based on the rate form of (14), supplemented with an equilibrium correction, the details of which can be found in Wu and Van der Giessen (1996), Tijssens et al. (2000) and Basu and Van der Giessen (2002).

The system of differential equations resulting from the finite element discretization of the energy balance from Basu and Van der Giessen (2002) are modified to include the heat flux vector $\boldsymbol{\mathcal{D}}_c$ from the crazing process

$$\boldsymbol{C}\dot{\boldsymbol{\Theta}}+\boldsymbol{D}\boldsymbol{\Theta}=\boldsymbol{\mathcal{D}}_b+\boldsymbol{\mathcal{D}}_c \tag{15}$$

Here, is the vector of nodal temperatures and $\boldsymbol{\mathcal{D}}_b$ is the heat source vector due to plastic dissipation in the bulk. The matrices $\boldsymbol{C}$ and $\boldsymbol{D}$ depend on the properties ρc_v and k, respectively. Equation (15) is integrated in time by an unconditionally stable central difference scheme and the same finite element mesh is used as for the mechanical part (14). The coupled problem is handled in a staggered manner.

5. Results

The aim of the present study is to give insight into the influence on fracture of the temperature elevation due to dissipation caused by both shear yielding in the bulk and by crazing. The material and craze parameters are reported in Tables 1–3.

As mentioned in Section 2, the parameters of the bulk in the glassy state are representative of SAN. These are adopted in the present numerical investigation as SAN

exhibits an intermediate response between the brittle PMMA and the ductile PC. The set of material parameters is supplemented with those of $\varkappa$ and m for the description above T_g in Equation (8). The parameters involved in the thermal part of the analysis for the estimation of the temperature dependence of the entanglement density and for the bulk conductivity are given in Table 2. These are copied from Basu and Van der Giessen (2002) and are thought representative to be for most glassy polymers . The values for the craze description are borrowed from the previous isothermal study (Estevez et al., 2000, case 8) because these were shown to be able to capture a ductile to brittle transition at low rates.

The range of loading rates where thermal diffusion needs to be considered is estimated through an argument (Basu and Van der Giessen, 2002) based on a one-dimensional problem. The following non-dimensional quantity κ compares a characteristic time scale t_0 associated with the loading conditions to the time for heat to diffuse over a characteristic length L_0 of the problem

$$\kappa = \frac{kt_0}{\rho c_v L_0^2}\,.$$

For $\kappa \gg 1$, isothermal conditions prevail while $\kappa \ll 1$ when the situation is adiabatic. The characteristic time scale t_0 for the present study is defined as the time to attain the material toughness K_I^{cr} for a given loading rate as $t_0 = K_I^{cr}/\dot{K}_I$. The toughness of amorphous polymer ranges from $1\,\mathrm{MPa}\sqrt{\mathrm{m}}$ for PMMA to $3 \sim 4\,\mathrm{MPa}\sqrt{\mathrm{m}}$ for PC under quasi-static conditions; for our estimate of t_0, we use $K_I^{cr} = 1\,\mathrm{MPa}\sqrt{\mathrm{m}}$. The characteristic length L_0 is taken to be the size of the plastic zone for perfectly plastic material, i.e. $L_0 \approx \left(K_I/\tau_y\right)^2$, in which τ_y is the yield stress of the bulk. The latter value can be obtained from pure shear tests at prescribed strain rates and temperatures, but a useful definition of the shear rate near the crack tip is ambiguous. For simplicity, we just use the high strain-rate, low temperature estimate $\tau_y \approx s_0$ so that $L_0 \approx (K_I/s_0)^2$.

For $\kappa \approx 1$, heat conduction needs to be accounted for. In terms of loading rate, this yields the estimate

$$\dot{K}_I = \frac{ks_0^4}{\rho c_v K_I^3} \approx 100\ \mathrm{MPa}\sqrt{\mathrm{m}}/\mathrm{s}$$

beyond which a coupled thermo-mechanical analysis is required. To illustrate the transition from isothermal to coupled thermo-mechanical conditions, loading rates of 30, 300 and $3 \times 10^3\,\mathrm{MPa}\sqrt{\mathrm{m}}/\mathrm{s}$ will be considered (values smaller than $30\,\mathrm{MPa}\sqrt{\mathrm{m}}/\mathrm{s}$ have already been investigated in Estevez et al. (2000)).

5.1. Reference case

For the lower loading rate of $30\,\mathrm{MPa}\sqrt{\mathrm{m}}/\mathrm{s}$, the calculated resistance curve is shown in Figure 4. The applied stress intensity factor is non-dimensionalized with s_0 and $\sqrt{r_t}$, and is plotted against the length of the craze L^c plus that of the crack length L^a (relative to the initial crack tip position) normalized with r_t. Three regimes are observed which are typical for the present model. The triangle indicates the onset of craze initiation when the condition (9) is fulfilled. When crazing initiates, the bulk

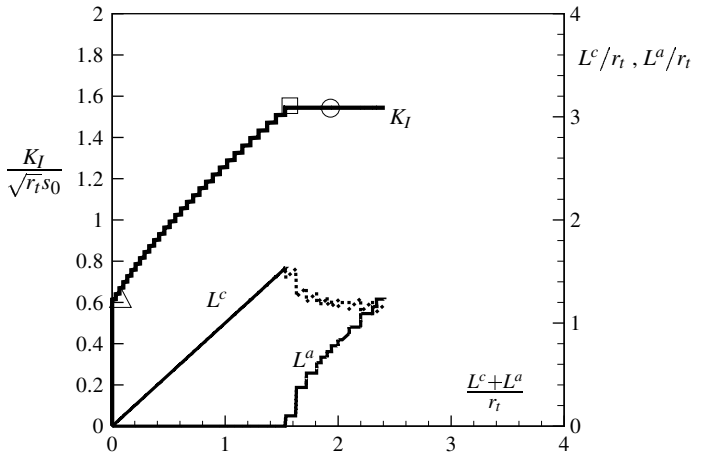

Figure 4. Crack growth resistance vs. craze length L^c plus crack length L^a for $\dot{K}_I = 30$ MPa$\sqrt{\text{m}}$/s. The triangle identifies the initiation of crazing, while the square marks the start of crack propagation after craze fibril breakdown. The circle marks a state during crack propagation, which is referred to in Figures 5 and 6.

response is elastic in this case and crazing nucleates at the crack tip. As the loading is further increased, crazing proceeds and due to the load-carrying capacity of the fibrils, some *R*-curve effect is observed. As the loading marked by the square is attained, the critical craze thickness $\Delta_{\text{n}}^{\text{ccr}}$ is reached at the tail of the craze and crack propagation starts. As the crack propagates, the resistance hardly increases, indicating the rather brittle response of the material. The level of the corresponding stress intensity factor is then taken as the critical toughness. Once crazing develops, the craze length L^{c} increases steadily until the condition for craze fibrils breakdown is attained. Then, crack propagation starts and L^{a} increases as the crack advances (Figure 4). At early stages of crack propagation, the craze length diminishes which corresponds to the breakdown of the first fibrils. Then, a stationary regime with a roughly constant craze length of about 100 μm during crack propagation is observed. Note that this craze length is obtained with a crack tip radius $r_{\text{t}} = 0.1$ mm and $\Delta_{\text{n}}^{\text{ccr}} = 10\mu$m (see Table 3). Reducing the crack tip radius and keeping the critical craze thickness the same did not change this prediction. On the other hand, reducing the critical craze thickness down to $\Delta_{\text{n}}^{\text{ccr}} = 3\mu$m results in a craze length of about 60–70 μm. For this range of parameters, the predicted craze length is consistent with the measured ones reported by Döll (1983; Döll and Könczöl, 1990).

Figure 5 shows the distributions of the plastic shear rate at the loadings marked by the square and the circle in Figure 4, i.e. at the onset of and during crack propagation. The plastic strain rate $\dot{\gamma}^{\text{p}}$ from (3) is normalized by $\dot{\Gamma}_0 = \dot{K}_{\text{I}} / \left(s_0\sqrt{r_{\text{t}}}\right)$, a reference strain rate at a distance r_{t} from the crack tip. Prior to crack propagation, it can be seen in Figure 5a that shear bands are active away from the crack symmetry plane rather than at the crack tip, due to the stress relaxation caused by crazing. During crack propagation (see Figure 5b), however, the plastic activity is concentrated around the crack–craze interface. At this stage, most of the deformation is accommodated by crazing while the bulk material behaves primarily elastic, thus resulting in a brittle response.

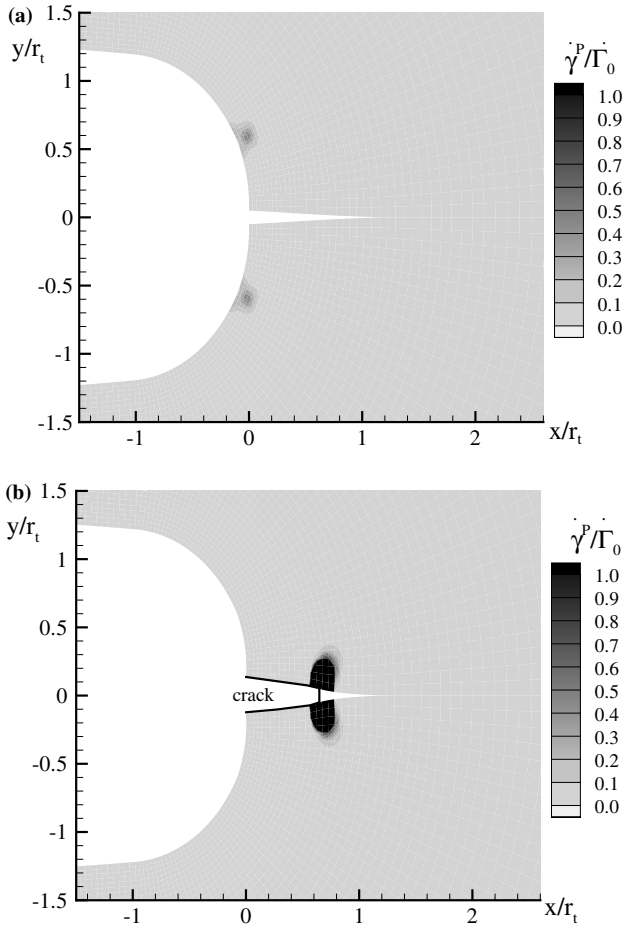

Figure 5. Plastic shear rate distribution (a) at the onset of crack propagation (square in Figure 4) and (b) during crack propagation (circle in Figure 4) for $\dot{K}_I = 30$ MPa$\sqrt{\text{m}}$/s.

The temperature distributions prior to and during crack propagation are reported in Figure 6. At the onset of craze initiation, no temperature change is observed as there is very little plastic deformation in this case. Prior to crack propagation (see Figure 6a), a slight increase of about 3K is observed at the crack tip, due to the craze viscoplasticity only. Heat generation is not observed from the emerging shear bands. Figure 6b shows the temperature distribution during crack propagation. The intense plasticity in the bulk around the crack–craze interface combined with craze thickening generates a heated zone along the crack path. The temperature increase is noticeable when the crack runs, but no toughening effect results from this temperature rise. Since the temperature remains unchanged during unstable crack propagation, the toughness found for the low loading rate with the thermo-mechanical analysis is identical to that found in the isothermal study (Estevez et al., 2000).

5.2. Temperature effects on shear yielding and craze thickening

Estevez et al. (2000) have shown that the fracture toughness is related to the competition between shear yielding and crazing, as expressed through their characteristic

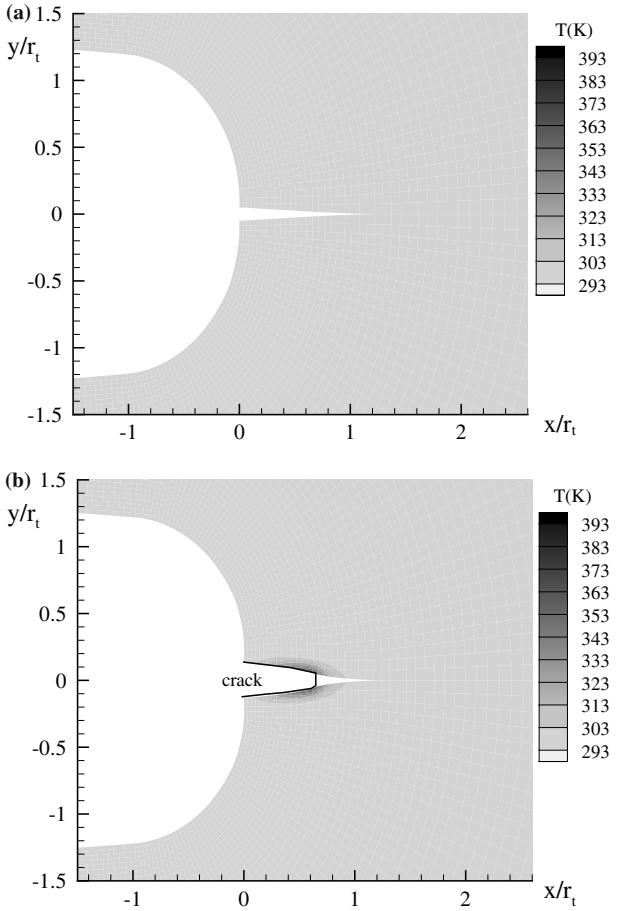

Figure 6. Temperature distribution (a) at the onset of crack propagation and (b) during crack propagation (corresponding to the square and circle in Figure 4, respectively) for $\dot{K}_I = 30\,\mathrm{MPa}\sqrt{\mathrm{m}}/\mathrm{s}$.

time scales. For instance, when crazing takes place, the condition for craze fibril breakdown defines the time t_c until crack propagation. This time scale can be defined through

$$\int_0^{t_c} \dot{\Delta}_n^c(T, \sigma_n)\mathrm{d}t = \Delta_n^{c\,cr}. \tag{16}$$

For a given loading rate $\dot{K}_I$, the viscoplastic craze thickening $\dot{\Delta}_n^c$ governs the time t_c till craze breakdown, and the related toughness as $K_I^{cr} = \dot{K}_I t_c$. Therefore, the toughness is not a material constant but is time and temperature dependent, which originates from the viscoplasticity of crazing.

Figure 7 gives the resistance curves obtained for increasing loading rates. The three regimes reported above for $\dot{K}_I = 30\ \mathrm{MPa}\sqrt{\mathrm{m}}/\mathrm{s}$ are seen to occur for higher rates as well. Craze initiation takes place at the loading level indicated by the triangle. In all cases shown, the bulk of the material is still elastic when the craze nucleates at the crack tip. The onset of crack propagation is marked with a square and

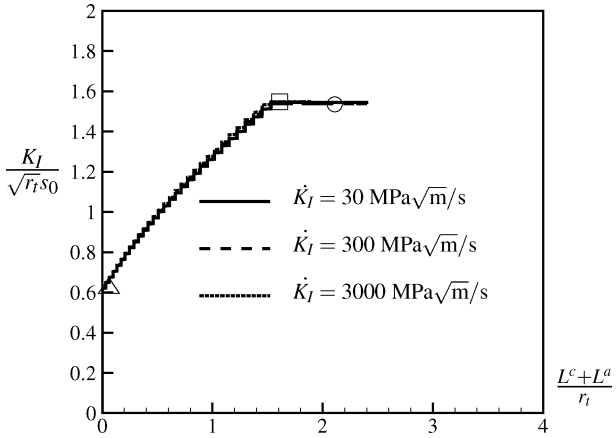

Figure 7. Resistance curves for loading rates increasing over two decades compared to the reference value of Figure 4. The onset of craze initiation is indicated by the triangle, the square shows when the condition for craze fibril breakdown is first encountered and the circle corresponds to the propagation of the crack, which takes place at a constant load used to define the material's toughness.

the loading level at this instant shows negligible variations with the loading rate, as does the length of the craze that has developed prior to crack propagation.

For the higher loading rates of $\dot{K}_I = 300$ MPa$\sqrt{\text{m}}$/s and 3000 MPa$\sqrt{\text{m}}$/s, the temperature distributions prior to crack propagation reported in Figure 8 shows that the maximum temperature increase is located near the original crack tip. This is where the craze has initiated and attained its maximum thickness. It appears that heat generated solely from the craze is responsible for the temperature rise along the craze faces. At this location, the temperature rise increases as the loading rate increases with a rise of 13 K for $\dot{K}_I = 300$ MPa$\sqrt{\text{m}}$/s (Figure 8a) and 40 K for $\dot{K}_I = 3000$ MPa$\sqrt{\text{m}}$/s (Figure 8b) at the onset of crack propagation. As the crack advances, plasticity occurs only at the crack–craze interface so that the heat generated from the craze thickening and from bulk yielding is responsible for the temperature increase as shown in Figure 9.

In order to check if crazing is the dominant heat source in the problem for these two loading rates, we have performed calculations in which crazing is suppressed so that heat generates only from the bulk. At the same load level as the crack started to propagate with crazing accounted for, Figure 10 shows the plastic strain rate distributions without crazing. For the two highest loading rates considered, shear bands have developed from yielding at the crack tip with a progressive expansion of the plastic zone characteristic of intrinsic softening materials as analyzed by Lai and Van der Giessen (1997). The plastic zone is slightly larger for the lowest loading rate since yielding takes place earlier during the loading history but with minor consequences for the plastic strain rate distribution. A noticeable temperature rise is observed for the highest loading rate of $\dot{K}_I = 3000$ MPa$\sqrt{\text{m}}$/s as reported in Figure 11. Its magnitude is about 10 K; a factor of four lower than that found with crazing (see Figure 8b). Apparently, crazing causes a stress relaxation which reduces the heat generation in the bulk. Since this heat source is already modest without crazing, heat generated by bulk viscoplasticity is probably negligible all together as soon as crazing takes place.

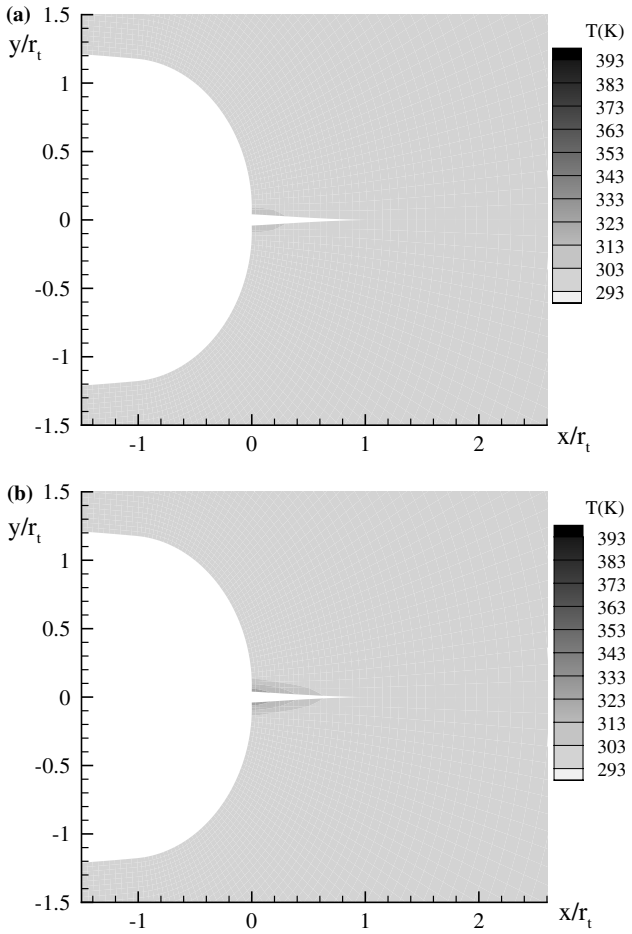

Figure 8. Temperature distribution prior to craze fibril breakdown marked by the square in Figure 7 for (a) $\dot{K}_I = 300$ MPa$\sqrt{\text{m}}$/s and (b) $\dot{K}_I = 3000$ MPa$\sqrt{\text{m}}$/s.

Thus, while a noticeable temperature increase can be observed prior to or during the early stages of crack propagation investigated here, no influence on the toughness is observed. Although the temperature increase prior to crack propagation can be up to 40 K, it has no consequences for crack growth. At this point, with the ingredients we put in the modeling, we are not able to predict any brittle-to-ductile transition as observed experimentally to occur in the loading range investigate here. The question if this may originate from the fact that we miss out on important temperature effects will be addressed in the next section.

5.3. Temperature-dependent craze initiation and breakdown

The fracture toughness determined by the onset of crack propagation depends on the competition between the kinetics involved in shear yielding and in crazing; or in other words, on how much energy has been dissipated when the condition for craze fibril breakdown is fulfilled. In the present study, we account for the influence of the temperature on this competition through the temperature dependence of plasticity of the bulk, Equation (3), and of the craze thickening rate, Equation (10).

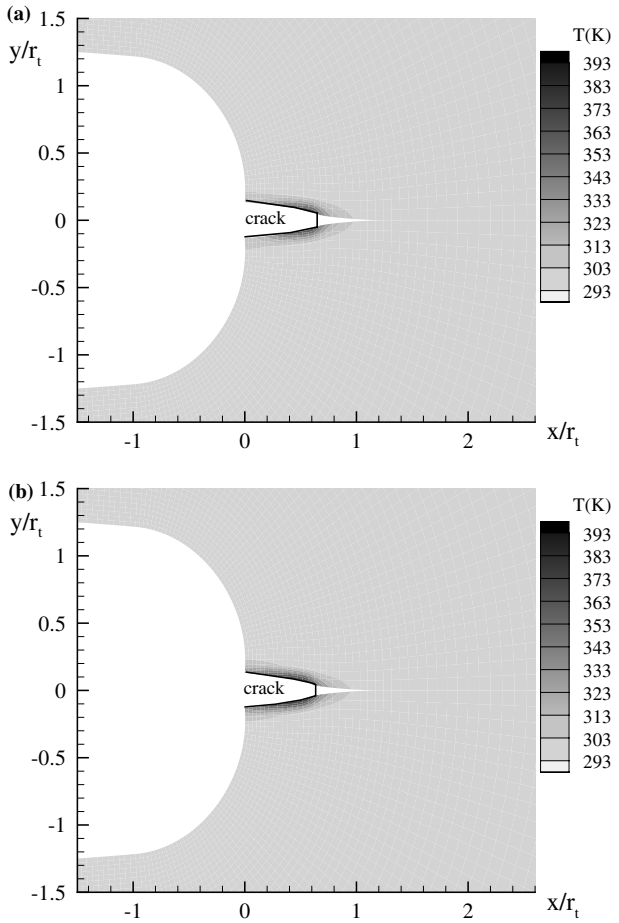

Figure 9. Temperature distribution during crack propagation marked by the circle in Figure 7 for (a) $\dot{K}_I = 300$ MPa$\sqrt{\text{m}}$/s and (b) $\dot{K}_I = 3000$ MPa$\sqrt{\text{m}}$/s.

At this point we have not considered the temperature dependence of craze initiation, which has been reported in (Sternstein and Myers, 1973). They have observed that craze initiation can be described by Equation (9) for temperatures above room temperature. There is no need to include this feature here since the temperature distributions presented above show that practically no heat is generated prior to craze initiation in all the cases analyzed.

The critical craze thickness is defined as a material parameter, which is primary dependent on the average molecular weight M_w. There are some conditions, however, where temperature effects on the critical craze thickness are observed. As reported in (Döll, 1983; Döll and Könczöl, 1990), there is a critical molecular weight M_w^{cr} below which no stable crazes are observed in glassy polymers. This corresponds to a vanishing Δ_n^{ccr} and a very brittle response. As the molecular weight is larger than M_w^{cr}, the critical craze thickness Δ_n^{ccr} can be considered approximately constant at a given temperature. However, for a material whose molecular weight is larger than this critical value, the critical craze thickness increases with temperature. Döll (1983) and Döll and Könczöl (1990) have investigated the critical craze thickness Δ_n^{ccr} of stable crazes

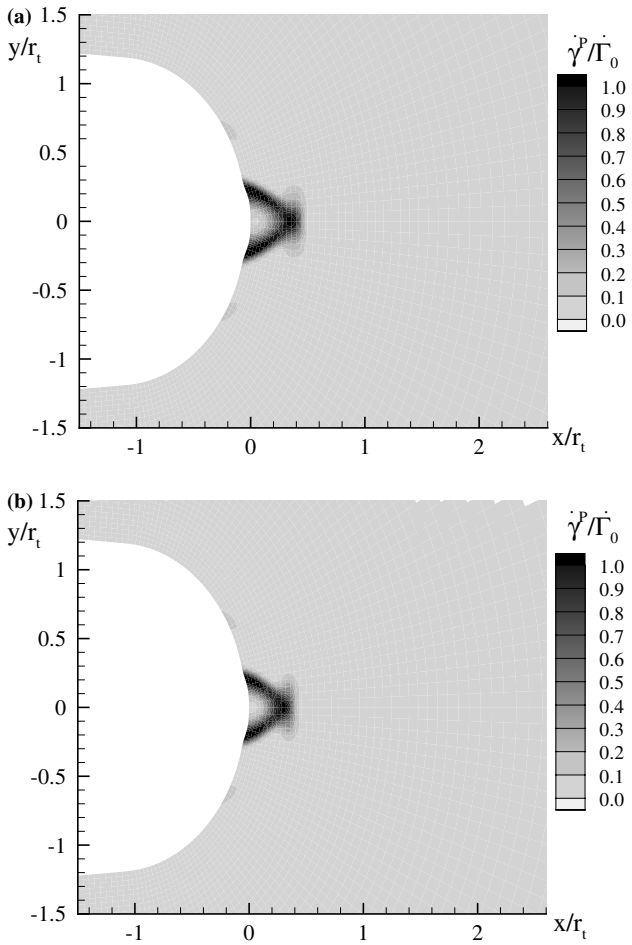

Figure 10. Plastic strain rate distributions at the critical toughness K_I^{cr} found in Figure 7, but without accounting for crazing for (a) $\dot{K}_I = 300$ MPa$\sqrt{\text{m}}$/s and (b) $\dot{K}_I = 3000$ MPa$\sqrt{\text{m}}$/s.

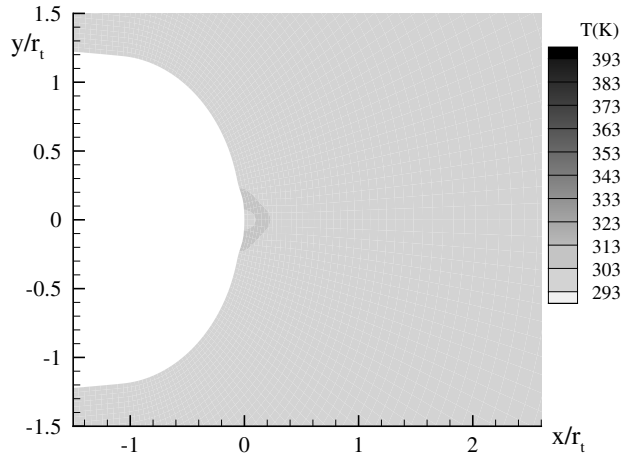

Figure 11. Temperature distribution at a loading corresponding to the critical toughness K_I^{cr} without accounting for crazing for $\dot{K}_I = 3000$ MPa$\sqrt{\text{m}}$/s.

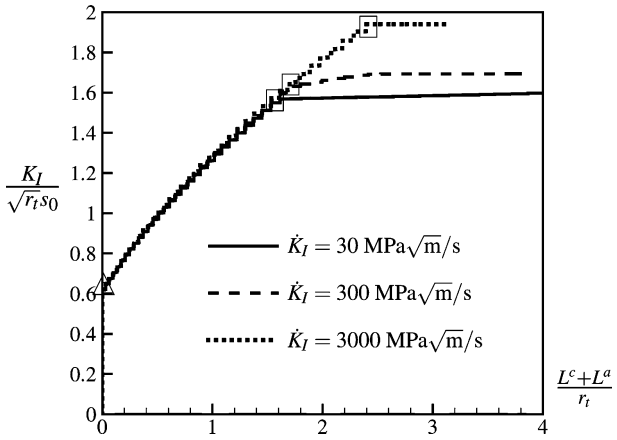

Figure 12. Resistance curves obtained with a temperature dependent critical craze thickness for $\dot{K}_I = 30, 300$ and 3000 MPa$\sqrt{\text{m}}$/s. The triangles indicate craze initiation and the squares indicate craze fibril breakdown.

in PMMA between 20°C and 70°C . They have observed that a factor of 1.5 can be found between the $\Delta_{\text{n}}^{\text{ccr}}$ at 20°C and 70°C for $M_{\text{w}} > 2 \times 10^6$g/mol. Since the glass transition temperature for PMMA is about 100°C, we now incorporate this effect in our analysis by assuming a linear temperature dependence of $\Delta_{\text{n}}^{\text{ccr}}$ from its value at room temperature (see Table 3) up to a two times larger value of $\Delta_{\text{n}}^{\text{ccr}} = 0.2 r_{\text{t}}$ at T_{g}.

Figure 12 shows the resistance curves for the three loading rates with this temperature dependence included. The curves are qualitatively similar to the ones in Figure 7 for a constant critical craze thickness, but the critical toughness is now observed to increase with increasing loading rate. For $\dot{K}_I = 30$ MPa$\sqrt{\text{m}}$/s, the toughness is almost identical to that obtained with a temperature-independent craze critical thickness. A small increase is already observed for $\dot{K}_I = 300$ MPa$\sqrt{\text{m}}$/s while it appears to be around 20% higher for $\dot{K}_I = 3000$ MPa$\sqrt{\text{m}}$/s.

For the two highest loading rates, the temperature increase due to the heat generated during crazing induces an increase of the craze critical thickness. The load carrying capacity of the craze is prolonged at the load level where craze fibril breakdown takes place with a constant $\Delta_{\text{n}}^{\text{ccr}}$. Thus, the onset of crack propagation is delayed so that a higher toughness is observed as reported in Figure 12 when compared to the cases in which a constant $\Delta_{\text{n}}^{\text{ccr}}$ is assumed (see Figure 7). Because of the same temperature effect, a small amount of crack growth resistance is observed for $\dot{K}_I =$ 300 MPa$\sqrt{\text{m}}$/s at early stages of crack propagation until $(L^{\text{c}} + L^a)/r_{\text{t}} = 2.4$. We can also notice that as $\Delta_{\text{n}}^{\text{ccr}}$ increases with temperature, the time t_{c} for craze fibril breakdown also rises so that more time is available for heat to diffuse. This promotes a slightly wider hot zone for $\dot{K}_I = 300$ MPa$\sqrt{\text{m}}$/s and $\dot{K}_I = 3000$ MPa$\sqrt{\text{m}}$/s which is also observed during crack propagation (see Figure 13).

6. Discussion

In the vicinity of the crack tip, the temperature observed prior to unstable crack propagation is noticeably enhanced for loading rates higher than $\dot{K}_I = 300$ MPa$\sqrt{\text{m}}$/s.

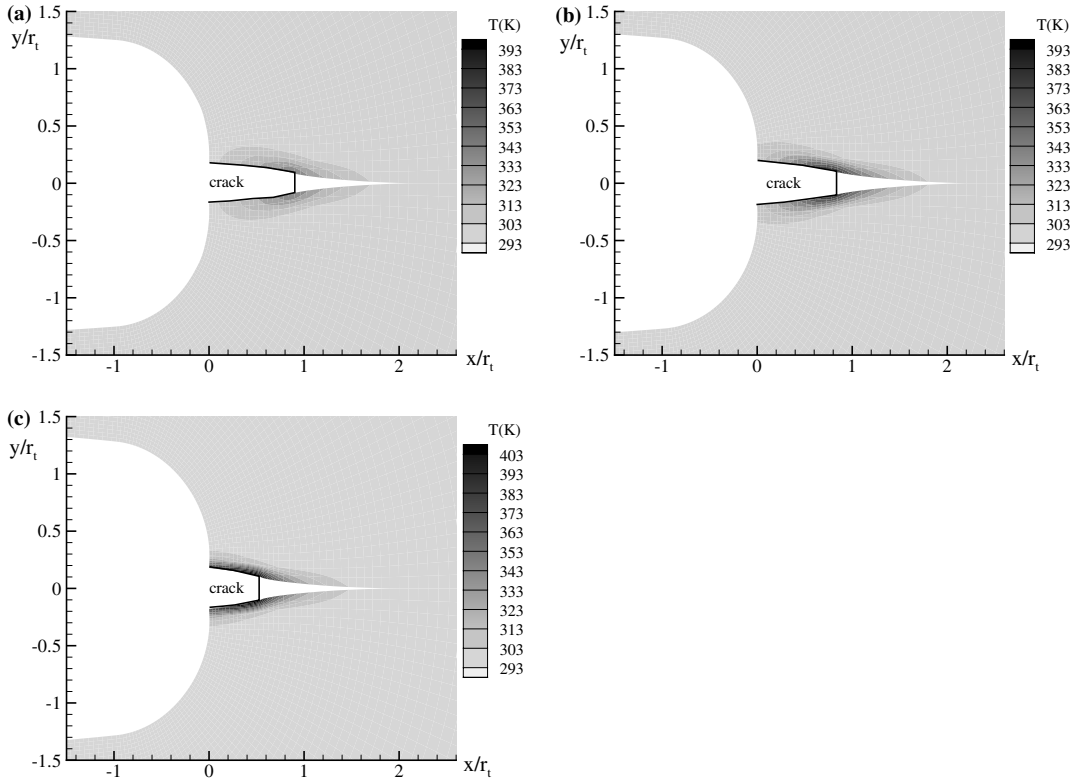

Figure 13. Temperature distribution during crack propagation for (a) $\dot{K}_I = 30$ MPa$\sqrt{\text{m}}$/s, (b) $\dot{K}_I = 300$ MPa$\sqrt{\text{m}}$/s and (c) $\dot{K}_I = 3000$ MPa$\sqrt{\text{m}}$/s, with a temperature dependent critical craze thickness. Compare with temperature-independent results in Figures 6, 9a and 9b, respectively.

The heat from craze thickening results in a hot zone along the craze surfaces, the extent of which is comparable to that of the craze thickness. In an experimental study of heat generated during the fracture of PMMA, Fuller et al. (1975) estimated the width of the hot zone along the crack path to be about one to three micrometers. The maximum craze thickness of PMMA reported by Döll (1983; Döll and Könczöl, 1990) is about two to three micrometers. Thus, although coming from different experiments, the size of the hot zone during crack propagation and the maximum craze thickness appear to be of the same order of magnitude. The corresponding quantities in our calculations are consistent with these observations. The heat originates primarily from craze thickening; the contribution from the bulk is negligible. This is demonstrated for $\dot{K}_I = 3000$ MPa$\sqrt{\text{m}}$/s in which a difference of factor four in the temperatures observed prior to crack propagation is observed when crazing is accounted for. The present observation is not restricted to static conditions. The minor importance of heat generated from the bulk for dynamic conditions has been demonstrated by Bjerke et al. (2002) for PC, which is considered as one of the most ductile glassy polymers. Thus, thermal effects come from craze thickening and the resulting hot zone along the craze surfaces extends over a few microns.

These observations tend to invalidate the interpretation by Williams and Hodgkinson (1981) of the marked increase of toughness with increasing loading rate. Their idea is

based on the assumption that crack propagation switches from isothermal to adiabatic conditions when the loading rate increases from static to dynamic conditions. Heat is assumed to originate from crazing and its diffusion around the craze surfaces is supposed to significantly reduce the yield stress of the bulk material surrounding the craze. Then, thermal effects are assumed to be large enough to promote plasticity in the bulk which results in blunting the crack. This picture has been named "thermal blunting" and some of its ideas can also be found in Fuller et al. (1975). However, this interpretation has been partially revoked by Williams and Adams (1987), who suggested that the toughness rise is due to dynamic effects. For loading rates at which inertia effects do not prevail, Williams and Adams (1987) caution that an interpretation in terms of thermal blunting or "some property variation" is to be considered.

One of such property variations, which we have studied here, is the possible variation of the critical craze thickness with temperature. Although the predicted toughness for $\dot{K}_I = 3000$ MPa$\sqrt{\text{m}}$/s is only about 20% larger than that with a constant craze critical thickness, it appears that, at least, this effect is to be accounted for up to loading rates at which crazing is observed while inertia effects do not prevail.

Results have not been reported for loading rates higher than 10^4 MPa$\sqrt{\text{m}}$/s. For these conditions, the glass transition temperature is reached during craze thickening, before the condition for craze fibril breakdown is attained. In this case, further craze thickening possibly involves a different mechanism than the one considered in Section 3 with localized plasticity at the craze–bulk interface. Other processes such as chain disentanglement or chain slippage may contribute to craze thickening and influence the toughness. Such a transition is not accounted for in the present study and would require a drastic modification of the crazing model.

For the quasi-static conditions investigated here, our description gives rise to a normal stress along the craze surface which is approximately constant during craze thickening. The level of the normal stress depends on the loading rate, so that our formulation resembles a visco-plastic strip model. In the predictions, the length of the craze is about hundred microns (see Figure 7) which is of the same order of magnitude as experimental data (Döll, 1983; Döll and Könczöl, 1990). From experiments on notched specimens of PMMA with various crack radii tested under three-point bending and tension, Elices et al. (2002) have identified a cohesive law with a constant traction zone to be suitable for capturing the experimental load vs notch opening displacement curves (also for static conditions). This is consistent with our findings.

Following the analysis of Bjerke et al. (2002) in which heat originating only from the bulk plasticity was accounted for, Bjerke and Lambros (2003) have investigated the temperature fields subsequent to heat generated during the *dynamic* failure of PMMA. They used the elastodynamic solution of a steady crack growth superposed with a cohesive zone description (Freund, 1990) to model the failure process. Various formulations of rate-independent cohesive zone laws were used together with the dissipation term $\sigma_c\dot{\delta}_c$, in which σ_c and $\dot{\delta}_c$ refer to the cohesive stress and opening displacement. The work $\sigma_c\dot{\delta}_c$ is considered as the only heat source. From the ultimate stress measured for tensile tests, they adopted a maximum stress of $\sigma_c = 120$ MPa for all cohesive zones. The maximum opening of the cohesive zones is derived from the value of σ_c and the measure of the energy release rate at different crack velocities. With these parameters, the heat flux can be estimated as in the present investigation

but Bjerke and Lambros (2003) defined an energy per unit volume by dividing $\sigma_c \dot{\delta}_c$ by an additional length H which represents the extent of material affected by the failure process of which radiation are measured. The temperature sensors are proportional to the radiating area so that the profile of the recorded temperature and the predictions can be compared.

It is worth noting that the predicted length (Bjerke and Lambros, 2003) of the cohesive zone is about 400 μm to 1 mm while that of a craze ahead of propagating cracks under quasi-static conditions is about or less than 100 μm (Döll, 1983; Döll and Könczöl, 1990). In order to interpret the discrepancy between Döll's data and their estimate of the craze length, Bjerke and Lambros (2003) pointed out that the cohesive zone of their analysis does not only represent crazing but the entire source of heat during crack propagation. Therefore, they argued that the cohesive zone accounts for the viscoplastic process of crazing but also includes thermal effects operating after fibrils break down, due to e.g. chain recoiling. These two contributions to heat are then lumped in the representative cohesive zone which would result in a length larger than that observed for crazing under static conditions. While a cohesive zone model for crazing at dynamic conditions is not available yet, the results of Bjerke and Lambros (2003) suggest the use of a formulation in which the normal stress reduces during thickening, which is different than the strip model used for static conditions. If two mechanisms are necessary to describe quasi-static and dynamic crazing, the switch from one to the other may contribute to the sharp transition reported in (Wada, 1992; Wada et al., 1996). More work on craze models is definitely needed.

Comments about the limitations of the present two-dimensional analysis are in place here. Craze initiation depends on the local level of hydrostatic stress (see Equation (9)) and its nucleation is enhanced if plane strain conditions prevail. Shear banding can be promoted under plane stress conditions if crazing does not nucleate. Such an influence has been observed experimentally by Inberg and Gaymans (2002) on PC with a noticeable decrease of the toughness with increasing specimen thickness. Thus, as the fracture toughness is primarily governed by the competition between crazing and shear yielding, a three-dimensional analysis may actually be required for a proper investigation of the relation between toughness and loading rate for real specimens.

A craze initiation criterion based on a critical stress state has been used so that the onset of crazing takes place at identical load levels for all loading rates as long as the bulk material is elastic. A time-dependent initiation criterion may be necessary under dynamic conditions since the characteristic time scale associated with the loading can be comparable to that involved in the craze nucleation process.

Thermo-elastic effects have not been considered since we first investigate the influence of the dissipative processes from shear yielding and crazing. In a study devoted to dynamic fracture of PMMA, Rittel (1998) shows that a cooling of about 30°C precedes crack propagation. It is generally thought that crazing operates for temperatures higher than the secondary transition temperature T_β. For PMMA or polystyrene this temperature coincides with the room temperature. Therefore, a thermo-elastic cooling as large as that reported by Rittel (1998) could inhibit crazing in these polymers and promote shear banding instead, resulting in a higher toughness.

The present study is restricted to a quasi-static formulation and focusses on the beginning of crack propagation. Our attention has been devoted to exploring possible causes for the onset of the brittle to ductile transition for such loading conditions. Therefore, arguments based on crack branching at high crack speed (as presented by Cotterell, 1965) are not considered and nor is a change from single to multiple crazing observed in the dynamic regime by Bjerke and Lambros (2003).

7. Conclusion

The present thermo-mechanical study extends a previous isothermal analysis (Estevez et al., 2000) to investigate loading rates for which thermal effects need to be accounted for, under quasi-static conditions. For the material parameters chosen here, the heat is shown to originate primarily from the craze thickening for loading rates higher than 300 MPa$\sqrt{\text{m}}$/s. The resulting hot zone affects the bulk material adjacent to the craze surfaces and extends over a distance comparable to that of the craze critical thickness. Despite the fact that shear yielding is temperature dependent, (1) the temperature increase is too localized to promote plasticity over a large area, and (2) thermal blunting is not seen.

The temperature dependence of the critical craze thickness has been shown to have a significant influence on toughness at loading rates in which thermal effects take place. The increase of K_I^{cr} is about 20% when compared to that with a constant critical craze thickness.

For loading rates above 10^4 MPa$\sqrt{\text{m}}$/s, the glass transition temperature is attained during craze thickening, prior to fibril breakdown and unstable crack propagation. For such conditions, the mechanism for craze thickening adopted here, with localized plasticity at the craze–bulk interface, becomes questionable. Further progress in the understanding of the brittle-to-ductile transition in amorphous polymers requires a better understanding and improved models for crazing.

Acknowledgments

The calculations reported on here were carried out at Montpellier's National Computer Centre of Higher Education (CINES, France) under Grant c20040922614/gep2443. Access to these facilities is gratefully acknowledged by R. Estevez.

References

Agassant, J.F., Avenas, P., Sergent, J.Ph. and Carreau, P.J. (1991). Polymer Processing: Principles and Modelling. Hanser Gardener Publications.

Argon, A.S. (1973). A theory for the low-temperature plastic deformation of glassy polymers. *Philosophical Magazine* **28**, 839–865.

Arruda, E.M. and Boyce, M.C. (1993). A three-dimensional constitutive model for large stretch behaviour of rubber elastic materials. *Journal of the Mechanics and Physics of Solids* **41**, 389–412.

Arruda, E.M., Boyce, M.C. and Jayachandran, R. (1995). Effects of strain rate, temperature and thermomechanical coupling on the finite strain deformation of glassy polymers. *Mechanics of Materials* **19**, 193–212.

Basu, S. and Van der Giessen, E. (2002). A thermo-mechanical study of mode I, small-scale yielding crack-tip fields in glassy polymers. *International Journal of Plasticity* **18**, 1395–1423.

Bjerke, T., Li, Z. and Lambros, J. (2002). Role of plasticity in heat generation during high rate deformation and fracture in polycarbonate. *International Journal of Plasticity* **18**, 549–567.

Bjerke, T.W. and Lambros, J. (2003). Theoretical development and experimental validation of a thermally dissipative cohesive zone model for dynamic fracture of amorphous polymers. *Journal of the Mechanics and Physics of Solids* **51**, 1147–1170.

Boyce, M.C., Parks, D.M. and Argon, A.S. (1988). Large inelastic deformation of glassy polymers. Part I: rate dependent constitutive model. *Mechanics of Materials* **7**, 15–33.

Boyce M.C. and Arruda E.M. (1990). An experimental investigation of the large strain compressive and tensile response of glassy polymers. *Polymer Engineering and Science* **30**, 1288–1298.

Cotterell, B. (1965). Velocity effects in crack propagation. *Applied Materials Research* **4**, 227–232.

Döll, W. (1973). An experimental study of the heat generated in the plastic region of a running crack in different polymeric materials. *Engineering Fracture Mechanics* **5**, 229–268.

Döll, W. (1976). Application of an energy balance and an energy method to dynamic crack propagation. *International Journal of Fracture* **12**, 595–605.

Döll, W. (1983). Optical interference measurements and fracture mechanics analysis of crack tip craze zones. *Advances in Polymer Science* **52–53**, 105–168.

Döll, W., Könczöl, L. (1990). Micromechanics of fracture: optical interferometry of crack tip craze zone. *Advances in Polymer Science* **91–92**, 138–214.

Elices, M., Guinea, G.V., Gómez, J. and Planas, J. (2002). The cohesive zone model: advantages, limitations and challenges. *Engineering Fracture Mechanics* **69**, 137–163.

Estevez, R., Tijssens, M.G.A. and Van der Giessen, E. (2000). Modeling of the competition between shear yielding and crazing in glassy polymers. *Journal of the Mechanics and Physics of Solids* **48**, 2585–2617.

Estevez, R., Basu, S. and Van der Giessen, E., (2000b). A thermo-mechanical investigation of the influence of shear yielding and crazing on fracture characteristics of glassy polymers. In: *Advances in mechanical behaviour, plasticity and damage* (Edited by D. Miannay, P. Costa, D. François, A. Pineau Euromat2000, Tours), pp. 233–238.

Freund L.B. (1990). Dynamic Fracture Mechanics. Cambrigde University Press, New York.

Fuller, K.N.G., Fox, P.G. and Field, J.E. (1975). The temperature rise at the tip of fast-moving cracks in glassy polymers. *Proceedings of the Royal Society of London* **A 341**, 537–557.

Haward R.N. and Young R.J. (1997). The physics of glassy polymers. 2nd edn., Chapman & Hall, London.

Inberg, J.P.F. and Gaymans, R.J. (2002). Polycarbonate and co-continuous polycarbonate/ABS blends: influence of specimen thickness, *Polymer* **43**, 3767–3777.

Ishikawa, M., Narisawa, I. and Ogawa, H. (1977). Criterion for craze nucleation in polycarbonate. *Journal of Polymer Science* **15**, 1791–1804.

Kambour, R.P. (1973). A review of crazing and fracture in thermoplastics. *Journal of Polymer Science, Macromolecular Reviews* **7**, 1–154.

Kramer, E.J. (1983). Microscopic and molecular fundamentals of crazing. *Advances in Polymer Science* **52–53**, 1–56.

Kramer, E.J. and Berger, L.L. (1990). Craze growth and fracture. *Advances in Polymer Science* **91–92**, 1–68.

Lai, J. and Van der Giessen, E. (1997). A numerical study of crack-tip plasticity in glassy polymers. *Mechanics of Materials* **25**, 183–197.

Lu, J. and Ravi-Chandar, K. (1999). Inelastic deformation and localization in polycarbonate under tension. *International Journal of Solids and Structures* **36**, 391–425.

Raha, S. and Bowden, P.B. (1972). Birefringence of plastically deformed PMMA. *Polymer* **13**, 174–183.

Rittel, D. and Maigre, H. (1996). An investigation of dynamic crack initiation in PMMA. *Mechanics of Materials* **23**, 229–239.

Rittel, D. (1998). Experimental investigation of transient thermoelastic effects in dynamic fracture. *International Journal of Solids and Structures* **35**, 2959–2973.

Rittel, D. (1999). On the conversion of plastic work to heat during high strain rate deformation of glassy polymers. *Mechanics of Materials* **31**, 131–139.

Robertson R.E. (1966). Theory for the plasticity of glassy polymers. *Journal of Chemical Physics* **44**, 3950–3956.

Steenbrink A.C. and Van der Giessen E. (1999). On cavitation, post-cavitation and yield in amorphous polymer-rubber blends. *Journal of the Mechanics and Physics of Solids* **47**, 843–876.

Sternstein, S.S. and Ongchin, L. (1969). Yield criteria for plastic deformation of glassy high polymers in general stress fields. *Polymer preprints* **10** (2), 1117–1124.

Sternstein, S.S. and Myers, F.A. (1973). Yielding of glassy polymers in the second quadrant of principal stress space. *Journal of Macromolecular Science-Physics* **B8** (3–4), 539–571.

Tijssens, M.G.A., Van der Giessen, E. and Sluys, L.J. (2000). Modeling of crazing using a cohesive surface methodology. *Mechanics of Materials* **32**, 19–35.

Van der Giessen, E. (1997). Localized plastic deformations in glassy polymers. *European Journal of Mechanics, A/Solids* **16**, 87–106.

Van Krevelen, D.W. (1990). Properties of Polymers. 3rd edn. Elsevier.

Wada, H. (1992). Determination of dynamic fracture toughness for PMMA. *Engineering Fracture Mechanics* **41**, 821–831.

Wada, H., Seika, M., Kennedy, T.C., Calder, C.A. and Murase, K. (1996). Investigation of loading rate and plate thickness effects on dynamic fracture toughness of PMMA, *Engineering Fracture Mechanics* **54**, 805–811.

Williams, J.G. and Adams, G.C. (1987). The analysis of instrumented impact tests using a mass-spring model. *International Journal of Fracture* **33**, 209–222.

Williams, J.G. and Hodgkinson, J.M. (1981). Crack-blunting mechanisms in impact tests on polymers. *Proceedings of the Royal Society of London* **A 375**, 231–248.

Wu, P.D. and Van der Giessen, E. (1993). On improved network models for rubber elasticity and their applications to orientation hardening in glassy polymers. *Journal of the Mechanics and Physics of Solids* **41**, 427–451.

Wu, P.D. and Van der Giessen, E. (1996). Computational aspects of localized deformations in amorphous glassy polymers. *European Journal of Mechanics, A/Solids* **15**, 799–823.